ORAL REFERENCE ICF100910OR

AN EXTENDED VOID GROWTH MODEL FOR DUCTILE FAILURE – ASSESSMENT FOR NON RADIAL LOADINGS AND APPLICATION TO FRACTURE TOUGHNESS PREDICTION

T. PARDOEN[1], L. COUSIN-CORNET[1], and J.W. HUTCHINSON[2]

[1]Université catholique de Louvain, Département des Sciences des Matériaux et Procédés, PCIM, Bâtiment Réaumur, 2 Place Sainte Barbe, 1348 Louvain-la-Neuve, Belgium
[2]Division of Engineering and Applied Sciences, Harvard University, Pierce Hall, Cambridge MA 02138, U.S.

ABSTRACT

An extended Gurson model incorporating the effects of the shape and spacing of the voids on the growth and coalescence is proposed. The onset of void coalescence is modeled as a transition from diffuse plasticity to transverse localized plastic yielding in the intervoid ligament. A simple constitutive model for the coalescence stage is also developed. An assessment of the model is proposed by comparison with void cell computations under non-radial loading conditions. The effect of the void shape on the fracture toughness is addressed using the assumption of uniaxial straining state within the fracture process zone. The analysis reveals that the effect of the void shape on the fracture toughness becomes significant for initial porosity larger than 10^{-4} and this effect increases for increasing initial porosity.

KEYWORDS

Fracture toughness, ductile fracture, ductility, metal alloys, void growth, void coalescence

INTRODUCTION

Recent efforts in the development of computational models incorporating the void growth process has given rise to robust predictive methods for crack propagation in ductile solids, e.g. [1,2,3,4,5]. Most of these works employed the constitutive model initially proposed by Gurson [6], improved by Tvergaard [7], and finally extended by Needleman and Tvergaard [8]. Although good agreement with a range of experiments and void cells computations has been observed, the model as it currently stands still suffers from limitations which are though to arise partly because (i) *void shape* is not directly accounted for and (ii) *void coalescence* is not properly modeled. Hence, an enhanced void growth model incorporating void shape, void distribution et void coalescence effects has been developed by integrating contributions by Gologonu [9], Thomason [10] and new ingredients related to strain hardening and to the final coalescence stage [11]. The axisymmetric version of the model has been extensively validated by comparisons with void cell simulations performed under constant stress triaxiality in Ref. [11]. This report addresses two issues. First, the void growth model is again assessed by comparison with unit cell calculations, in the case of a constant strain biaxiality ratio. This mode of loading allows analyzing the pertinence of the model under non-radial loading. In the second part, the extended void growth model is used to draw qualitative features about the effect of void shape and void distribution on the fracture toughness of metal alloys.

Summary of the model. Only axisymmetric stress states are considered in the present work and the solid is made of a periodic distribution of the cylindrical representative volume element (RVE) defined on Fig. 1.

Void growth model. The extension of the Gurson model due to Gologanu *et al.* [9], which has been adopted here to describe behavior prior to void coalescence, gives a constitutive relation for a porous elastoplastic material containing (axisymmetric) spheroidal voids. This particular model, extended for strain-hardening, contains as state variables: the components of the mesoscopic stress tensor, $\boldsymbol{\Sigma}$, the porosity, f, the void aspect ratio, S, and an average yield stress for the matrix material, σ_m. The void aspect ratio is defined by $S = \ln(W)$ while $W = R_z/R_r$.

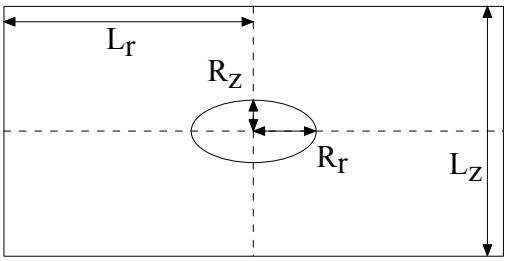

Figure 1: Representative volume element

The functional form of the model prior to coalescence is:

$$\Phi \equiv \Phi(\boldsymbol{\Sigma}, f, S, \sigma_m) = 0, \tag{1}$$

$$\dot{f} = (1-f)\dot{E}^p_{kk}, \tag{2}$$

$$\dot{S} \equiv \dot{S}(f, S, T), \tag{3}$$

$$\sigma_m \dot{\varepsilon}^p_m (1-f) = \Sigma_{ij} \dot{E}^p_{ij}, \tag{4}$$

$$\sigma_m \equiv \sigma_m(\varepsilon_e), \tag{5}$$

$$\dot{E}^p_{ij} = \gamma \frac{d\Phi}{d\Sigma_{ij}}, \tag{6}$$

where Φ is the flow potential; $\boldsymbol{E}^p$ is the mesoscopic plastic strain tensor; (2) and (3) are the evolution laws for f and S, respectively; (4) is the Gurson [6] energy balance for the plastic work allowing computation of σ_m using the effective stress-strain curve for the parent material (5); and (6) is the flow rule. The expressions for the functions such as Φ and the evolution of S are given in Ref. [9,11].

Criterion for the onset of void coalescence. Axisymmetric void cell computations [11,12] have shown that void coalescence consists in the localization of plastic deformation in the ligament between the voids, which, experimentally, gives rise to a flat dimpled fracture surface. Thomason [10] has studied the transition to localization for elastic-perfectly plastic solids by looking at artificially constrained localized solutions giving the load as a function of the void cell geometry. For axisymmetric geometry, Thomason has proposed that the average normal stress acting on the cell at the onset of localization occurs when Σ_z attains Σ_z^{loc} where

$$\frac{\Sigma_z^{loc}}{\sigma_0} = \left[1 - \left(\frac{R_r}{L_r}\right)^2\right]\left[\alpha\left(\frac{R_z}{L_r - R_r}\right)^{-2} + \beta\left(\frac{R_r}{L_r}\right)^{-1/2}\right], \tag{7}$$

where $\alpha = 0.1$ and $\beta = 1.2$. By comparing this expression with our numerical results for strain hardening materials [11], we also find that this expression provides an accurate estimate for the onset of localization within the cells, provided that σ_0 is replaced by an appropriate effective flow stress for the matrix, σ_m (see also [13]), and α and β incorporate a dependence on the strain hardening exponent n. The effective matrix stress, σ_m, is obtained using (4) and (5). A fitting procedure performed on a large number of void cell results [9] has revealed that the coefficient β is almost constant equal to 1.24 while $\alpha(n) = 0.1 + 0.22n + 4.8\,n^2$ ($0 \le n \le 0.3$). With relation (7), a new geometrical variable related to the void spacing has entered the model. For the sake of simplicity in the formulation of the model, we have chosen to use $A = \ln(\lambda) = \ln(L_z/L_r)$. The model thus depends on all the geometric characteristics of the representative void cell: f, A (or λ), S (or W).

In [11], the criterion (8) has proved to very accurately predict the onset of coalescence for porosity ranging between 10^{-2} and 10^{-4}, stress triaxialities between 1/3 and 5, void shapes W between 1/6 and 6, and void distribution λ between 1/2 to 16.

A model for the post-localization regime. Relation (7) still pertains after the onset of coalescence and Σ_z^{loc} is replaced by Σ_z, assuming the voids do not depart significantly from a spheroidal shape. The additional equations for the evolution of the state variables during the post-localization stage are obtained under the approximation that elasticity, as well as any reversed plasticity, are neglected. In agreement with the void cell results, the half-height of the localization zone is approximated as R_z (i.e. $h = R_z$, see Fig. 1).

ASSESSMENT OF THE VOID GROWTH MODEL FOR NON-RADIAL LOADINGS

The predictions of the void growth model under constant applied strain biaxiality ratio are compared to finite element void cell simulations performed with the same applied biaxiality ratio. Results are presented for a material with $f_0 = 10^{-2}$, $\lambda_0 = 1$, $\sigma_0/E = 0.002$, $n = 0.1$ and $W_0 = 1/6$, 1, 6. The strain biaxiality ratio $\beta = E_r/E_z$ ranges from –0.5 to 0. As the applied boundary conditions prevent plastic tensile localization, the void coalescence model has been turned off except for the uniaxial straining case (β=0). Thick lines correspond to the unit cell calculations and thin lines correspond to the model predictions. Figures 2 show the variations with overall straining of different quantities computed with the void growth model and with the finite element unit cell computations for initially spherical voids (W_0=1) : the overall axial stress in (a), the porosity in (b) and the void shape in (c). Figures 3 shows the variation of the overall axial stress as a function of the overall axial strain for voids initially (a) very oblate (W_0=1/6) or (b) very prolate (W_0=6).

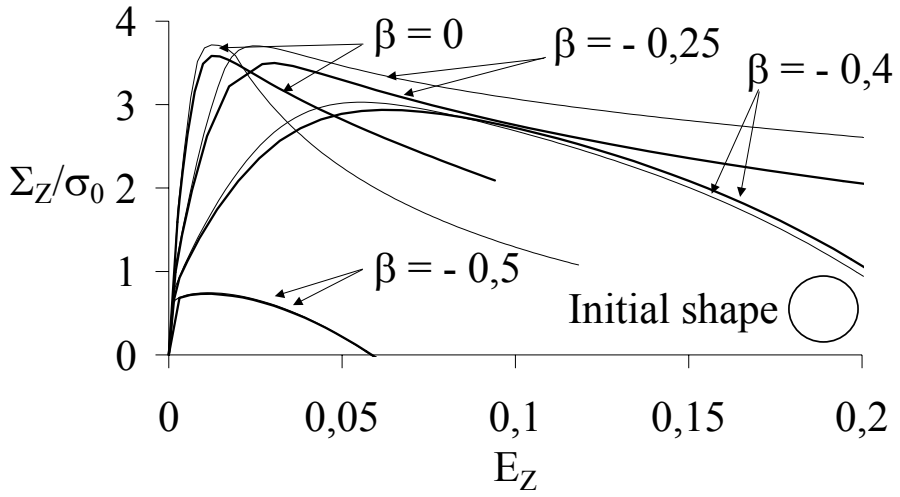

(a)

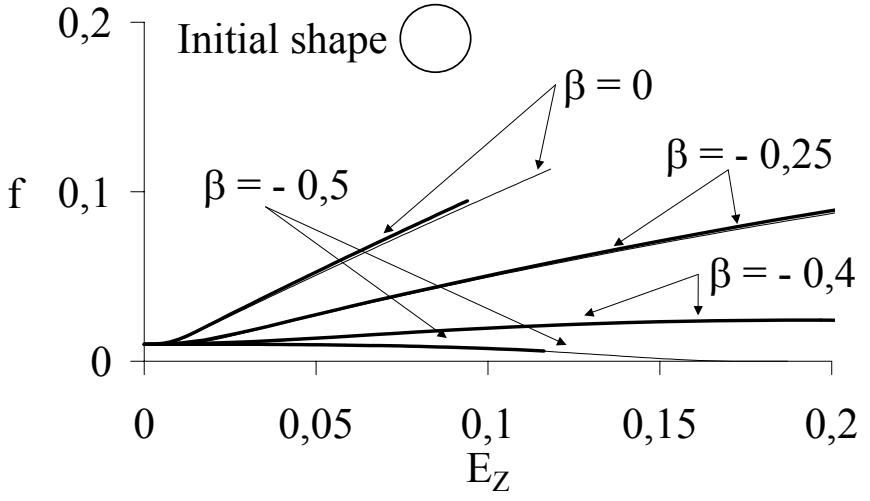

(b)

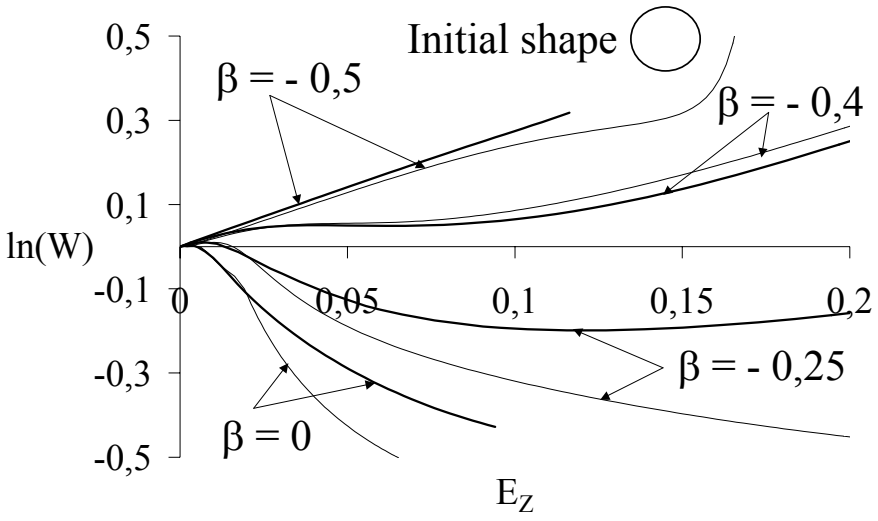

(c)

Figure 2: Variation as a function of the overall axial strain of (a) the overall axial stress, (b) the porosity, and (c) the void shape, for a material characterized by $f_0 = 10^{-2}$, $\lambda_0 = 1$, $\sigma_0/E = 0.002$, $n = 0.1$ and $W_0 = 1$.

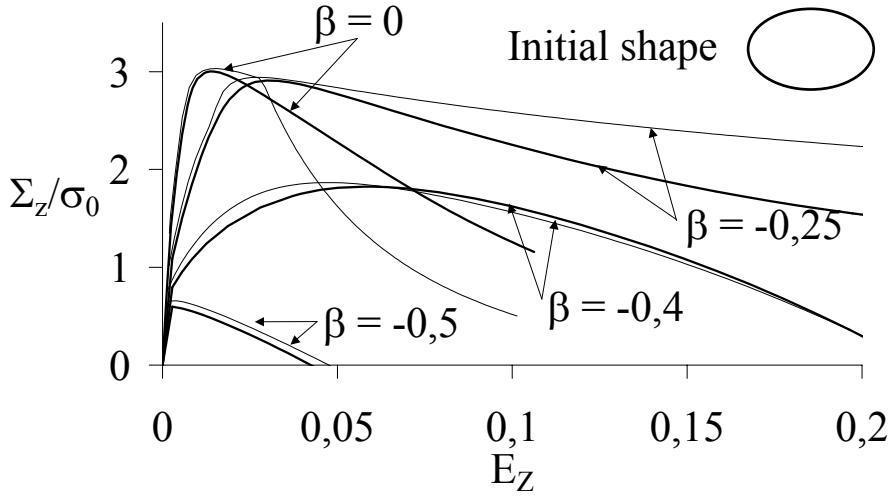

(a)

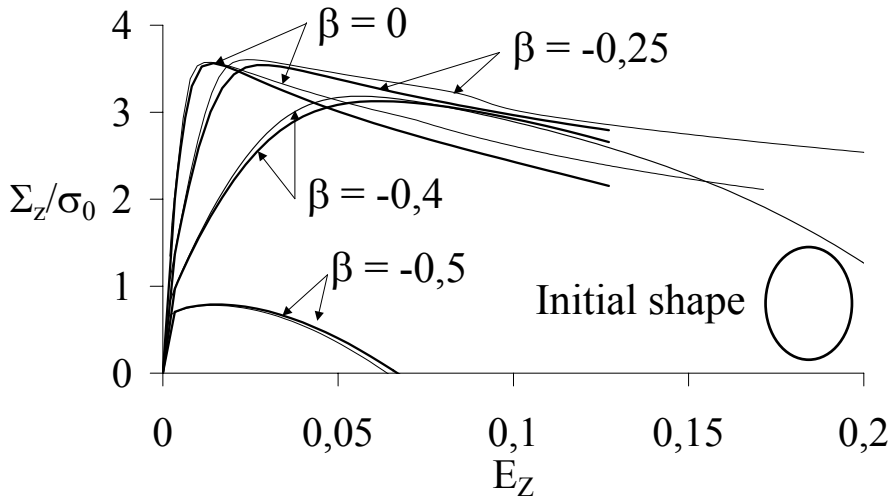

(b)

Figure 3: Variation of the overall axial stress as a function of the overall axial strain for a material characterized by $f_0 = 10^{-2}$, $\lambda_0 = 1$, $\sigma_0/E = 0.002$, $n = 0.1$ and (a) $W_0 = 1/6$ and (b) $W_0 = 6$ (a).

Figs. 2a and Figs. 3 show that the overall stress-strain behavior obtained with the model quantitatively agrees with the finite element unit cell solution. The most important characteristics, which are the maximum stress (the "strength" of the material) and the strain at final fracture (the "ductility" of the material), are predicted with an accuracy increasing when the strain biaxiality decreases. One should note that a constant strain biaxiality ratio involves marked variations of the stress triaxiality during deformation. In the case of large strain biaxiality ratio, the stress triaxiality sometimes reaches values larger than 5 or 6 for which other phenomena, such as unstable void growth may be expected.

FRACTURE TOUGHNESS PREDICTION

As initially proposed by Andersson [14] and then revisited by Tvergaard and Hutchinson [15], the fracture process zone at the tip of a sharp crack can be anticipated as a row of multiple interacting voids which, to a good approximation, are strained uniaxially during the major part of the void growth. Indeed, under large stress triaxiality, the fracture process involves early localization of the plastic flow in a planar zone of essentially one void spacing in thickness. Assuming spherical voids and isotropic void distribution, Tvergaard and Hutchinson [15] have shown that the fracture toughness, J_{Ic}, governing crack growth initiation can almost exactly be expressed as

$$J_{Ic} = \Gamma_0 \tag{9}$$

where Γ_0 is the work per unit area spent in the band until final failure. It can be computed from the Gurson model according to

$$\frac{\Gamma_0}{\sigma_0 L_{r0}} = F\left(\frac{\sigma_0}{E}, n, f_0\right) \tag{10}$$

where E is the Young's modulus. Xia and Shih [16] have shown that the uniaxial straining assumption is valid as long as f_0 is not too small. Typically, when f_0 becomes smaller than 0.1%, a one void - crack interaction mechanism takes place. In that case, the uniaxial straining assumption looses its pertinence. The analysis of Tvergaard and Hutchinson [15] has been extended by accounting for the effect of the void shape using the extended-Gurson model. Now, F generally writes $F = F(\sigma_0/E, n, f_0, W_0)$, assuming isotropic initial void distribution ($\lambda_0 = 1$). This extended model allows addressing the anisotropic fracture toughness of metal alloys. Indeed, since it accounts for the void shape, this model is able to capture variations of the fracture toughness with the orientation of the crack plane resulting from preferential orientation of the inclusions.

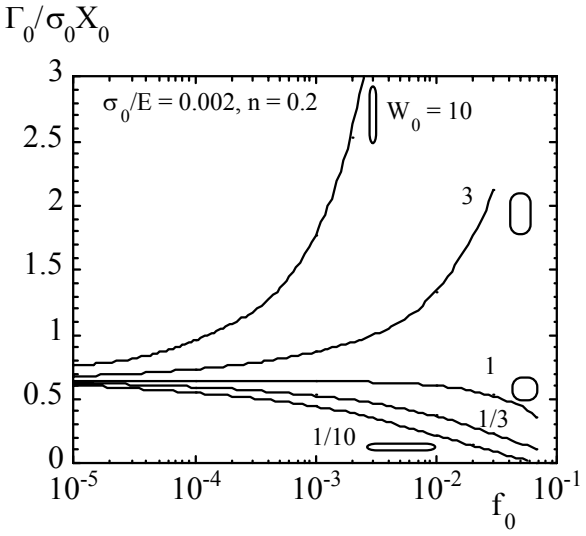

Figure 4: Variation of $F = \Gamma_0/\sigma_0 L_{r0}$ as a function of the initial porosity f_0 for various initial void shape

The variation of $\Gamma_0/\sigma_0 L_{r0}$ as a function of the initial porosity for various void shapes is shown in Fig. 4 (for n = 0.2 and σ_0/E = 0.002). The effect of the initial void shape is significant for porosity larger than about 10^{-4}. Prolate shape increases $\Gamma_0/\sigma_0 L_{r0}$ while oblate shape reduces it. For void shape departing from spherical,

$\Gamma_0/\sigma_0 L_{r0}$ cannot be considered anymore as independent of the initial porosity, it increases with f_0 for prolate voids and decreases with f_0 for oblate voids.

The results of Fig. 4 can be used to qualitatively understand and predict the variation of the fracture toughness as a function of the loading direction for rolled plates with preferential orientation of the second phase. From these results it is concluded that void shape effects (and the combined effect coming from the change in ligament length) can alone explain a factor two (or more) difference in the toughness of plates with elongated inclusions depending on the orientation of the crack plane. Note that this analysis is only qualitative because of the assumed axisymmetry. In other words, a 90° rotation of a prolate void with $W_0 = a$ does not give an oblate void with $W_0 = 1/a$.

CONCLUDING REMARKS

The new model only depends on the initial values of the state variable and thus avoids the use of critical porosities (for the onset of coalescence and for final separation). The two additional microstructural characteristics of the new model, the void initial shape S_0 and the initial void distribution λ_0, can be obtained from the same metallographic analysis performed to ascertain f_0 and L_0. The comparison with the void cell simulations in Ref. [11] for constant stress triaxiality and, in this report, for constant strain biaxiality has established that the full void growth/coalescence model is able to quantitatively account for variations of all the characteristic parameters of the representative volume element of Fig. 1: porosity, void shape, cell aspect ratio, stress triaxiality, for a wide range of matrix flow behavior. Consequently, the model naturally allows addressing issues such as the anisotropy in fracture toughness observed in many materials formed with large amounts of plastic strains. Most importantly, behavior at low and large stress triaxiality are adequately encompassed by the same model, giving thus the possibility to deal with failure of thin and thick structural parts within the same framework.

ACKNOWLEDGEMENTS

The work of JWH was supported in part by the NSF grant CMS-9634632 and in part by the Division of Engineering and Applied Sciences, Harvard University. This work was carried out in the framework of program PAI41 supported by SSTC Belgium.

REFERENCES

1. Mudry, F., di Rienzo, F., and Pineau, A., (1989). In: *Non-Linear Fracture Mechanics: Volume II - Elastic-Plastic Fracture*, ASTM STP 995, pp. 24-39, Landes, J.D., Saxena, A., and Merkle, J.G. (Eds). American Society for Testing and Materials, Philadelphia.
2. Xia, L., Shih, C.F., and Hutchinson, J.W. (1995). *J. Mech. Phys. Solids* **43**, 389.
3. Brocks, W., Klingbeil, D., Kunecke, G., and Sun, D.-Z. (1995). In: *Constraint Effects in Fracture Theory and Applications: Second Volume*, ASTM STP 1244, pp. 232-252, Kirk, M. and Bakker, A. (Eds). American Society for Testing and Materials, Philadelphia.
4. Ruggieri, C., Panontin, T.L., and Dodds, R.H., Jr. (1996). *Int. J. Fract.* **82**, 67.
5. Gao, X., Faleskog, J., and Shih, C.F. (1998). *Int. J. Fract.* **89**, 374.
6. Gurson, A.L. (1977). *J. Engng. Mater. Tech.* **99**, 2.
7. Tvergaard, V. (1981). *Int J. Fract*. **17**, 389.
8. Needleman, A. and Tvergaard, V. (1984). *J. Mech. Phys. Solids* **32**, 461.
9. Gologanu, M., Leblond, J.-B., Perrin, G., and Devaux, J. (1995). In: *Continuum Micromechanics*, Suquet, P. (Ed.). Springer-Verlag.
10. Thomason, P.F. (1990) *Ductile Fracture of Metals*, Pergamon Press, Oxford.
11. Pardoen, T. and Hutchinson, J.W. (2000) *J. Mech. Phys. Solids* **48**, 2467.
12. Koplik, J. and Needleman, A. (1988). *Int. J. Solids Struct.* **24**, 835.
13. Zhang, Z. L. and Niemi, E. (1994). *Engng. Fract. Mech.* **48**, 529.
14. Andersson, H. (1977). *J. Mech. Phys. Solids* **25**, 217.
15. Tvergaard, V. and Hutchinson, J.W. (1992) *J. Mech. Phys. Solids* **40**, 1377.
16. Xia, L. and Shih, C.F. (1995). *J. Mech. Phys. Solids* **43**, 1953.